

## Relocation dynamics of domain boundaries in semiconductor superlattices

M. Rogozia,<sup>1</sup> S. W. Teitsworth,<sup>2</sup> H. T. Grahn,<sup>1,\*</sup> K. H. Ploog<sup>1</sup>

<sup>1</sup>*Paul-Drude-Institut für Festkörperelektronik, Hausvogteiplatz 5–7, 10117 Berlin, Germany*

<sup>2</sup>*Department of Physics, Duke University, Box 90305, Durham, North Carolina 27708-0305*

(Received 23 August 2001; revised manuscript received 7 December 2001; published 24 April 2002)

The formation of static electric-field domains in doped semiconductor superlattices appears in the current-voltage ( $I$ - $V$ ) characteristics as multiple current branches separated by abrupt discontinuities. The switching dynamics of the charge-accumulation layer forming the domain boundary is experimentally investigated at dc voltages in the first plateau of the  $I$ - $V$  characteristic for different polarities and amplitudes of the applied voltage steps. When the voltage is decreased (down jumps) from its initial dc value, the accumulation layer can directly move from its initial position to its final position, in accordance with the direction of the applied voltage step. However, when the voltage is increased (up jumps), there are two different modes of the relocation motion of the accumulation layer. For small up jumps, the accumulation layer can still move directly from its initial to its final position. When the amplitude of the transient current peak is above a critical value, a charge dipole is injected at the emitter contact, in addition to the existing monopole formed by the domain boundary. The experimentally observed switching behavior is in excellent qualitative agreement with recent theoretical work [A. Amann *et al.*, Phys. Rev. E **63**, 066207 (2001)].

DOI: 10.1103/PhysRevB.65.205303

PACS number(s): 73.50.Fq, 05.60.-k, 73.61.Ey

### I. INTRODUCTION

The current-voltage ( $I$ - $V$ ) characteristics of highly doped, weakly coupled superlattices (SL's) exhibit as many well-defined branches on each current plateau as there are periods in the SL due to the formation of static electric-field domains.<sup>1</sup> Two adjacent branches are separated by a discontinuity in the current. Under domain formation, the spatial distribution of the electric field inside the SL breaks up into two domains, which are separated by a domain boundary in the form of a charge accumulation layer (CAL). The domain boundary is essentially confined to a single SL period, i.e., to one quantum well of the SL, since the SL is weakly coupled so that charge can only reside in the wells and not in the barriers. The low-field domain consists of a region of a lower uniform electric field on the injecting contact side forming the emitter of the SL, while the high-field domain is formed by a region of a higher uniform electric field on the receiving contact side representing the collector (cf. Fig. 1). When the applied bias sweeps across a discontinuity from one current branch to the next, the domain boundary moves exactly by one SL period.<sup>2</sup> Early experimental<sup>3,4</sup> and theoretical<sup>5</sup> studies of the domain formation process and its time constant examined the time it takes for the domain boundary to reach its steady-state position after applying a certain voltage step to an initially *unbiased* SL.

Later, switching experiments investigating the relocation dynamics of the domain boundary over one or several periods were performed by Luo *et al.*<sup>6</sup> The transition process from one branch to the next was studied by adding a bias step with different amplitudes to a dc bias and recording the time-resolved current. It was shown that the relocation time of the domain boundary for up jumps (down jumps) depends exponentially on the difference between the final static current and the maximum (minimum) current value of the initial branch, which is reached before the relocation of the domain boundary takes place. A universal relationship between the

relocation time and the current difference was found.

More recently, we experimentally investigated the probability distribution function of the relocation time for up jumps to the adjacent branch close to the discontinuity in the  $I$ - $V$  characteristic.<sup>7</sup> The mean value of the relocation time increases by more than one order of magnitude, when the final voltage on the adjacent branch is reduced to a value approaching the discontinuity. At the same time, the distribution function of the relocation time changes from a Gaussian to a first-passage time form.

Very recent theoretical investigations describe the upstream motion of CAL's,<sup>8</sup> the dynamic scenarios of multistable switching,<sup>9,10</sup> and the general motion of CAL's<sup>11</sup> in semiconductor SL's. Under certain conditions, it was predicted that the domain boundary can move upstream against the flow of electrons. For appropriate doping concentrations, the CAL moves downstream for current values below a certain critical current, remains stationary between this value and a second critical current, and moves upstream for values above the second critical current.<sup>8</sup> The numerical analysis of the switching between different branches using the sequential-resonant-tunneling model results in several switching scenarios depending on the direction and amplitude of the applied voltage steps.<sup>9,10</sup> For any voltage de-

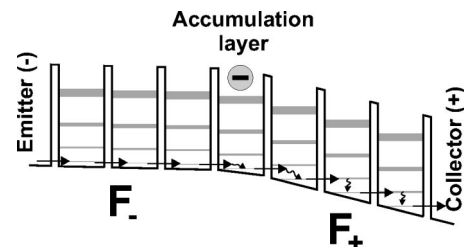


FIG. 1. Schematic diagram of the distribution of the low ( $F_-$ ) and high ( $F_+$ ) electric-field domain in a weakly coupled SL. The domain boundary is formed by the accumulation layer.

crease (down jumps) as well as for a small voltage increase (up jumps) in the first current plateau, the relocation of the domain boundary will always occur by a direct movement of the charge monopole forming the domain boundary to its final position. However, for larger up jumps, a charge dipole is injected at the emitter contact in addition to the existing monopole formed by the domain boundary, since the monopole alone cannot move upstream over several periods. Furthermore, the transient behavior from an unstable point to a stable point in the current-voltage characteristics, after a steplike or ramplike increase of the external voltage, was theoretically investigated. Finally, recent theoretical work discussed the effects of different doping levels on possible types of CAL motion in semiconductor SL's.<sup>11</sup>

In this paper, a complete picture of the relocation dynamics, involving deterministic and stochastic mechanisms, is inferred from experimental investigations and compared to recent theoretical predictions. The different relocation scenarios depend on the direction and amplitude of the applied voltage steps, the interplay between deterministic and stochastic processes, the ramp time of the voltage, and the sweep rate. For down jumps, we always observe a direct monopole relocation. For small up jumps, the domain boundary can actually move upstream, so that the relocation scenario is similar to that for down jumps. However, for larger up jumps, i.e., when the amplitude of the transient current peak is above a critical value, the system no longer supports the upstream motion of the monopole, and a dipole is injected from the emitter in addition to the already existing monopole. The motion of this combined system of a monopole and a dipole is rather complex, and will be described in detail. The critical current level depends on the relation between the contact resistance and the effective drift velocity characteristic of the SL.

After describing the experimental details in Sec. II, the current-voltage characteristics are presented in Sec. III. In Sec. IV, the down jumps, which always occur via a simple monopole relocation, are discussed. Section V deals with up jumps, which can be described by monopole (for small up jumps) and *tripole* relocation (for large up jumps). Section VI describes the transient response of the current to gradually ramped voltage steps and triangular voltage sweeps. Finally, the main results of the paper are summarized in Sec. VII.

## II. EXPERIMENTAL DETAILS

The investigated SL consists of  $N_{\text{SL}} = 40$  periods of 9-nm-wide GaAs wells and 4-nm-wide AlAs barriers grown by molecular-beam epitaxy. The central 5 nm of each well are Si doped with a density of  $3 \times 10^{17} \text{ cm}^{-3}$ , corresponding to a sheet concentration of  $N_D = 1.5 \times 10^{11} \text{ cm}^{-2}$  per well. The SL is sandwiched between two highly doped  $\text{Al}_{0.5}\text{Ga}_{0.5}\text{As}$  contact layers, which act as window layers in order to have optical access to the SL structure.<sup>12,13</sup> The sample is supplied with Ohmic contacts, etched into mesas with a diameter of  $120 \mu\text{m}$ , and mounted on a sapphire holder in a He-flow cryostat equipped with 20-GHz coaxial cables. All reported measurements are performed at a temperature of 5 K.

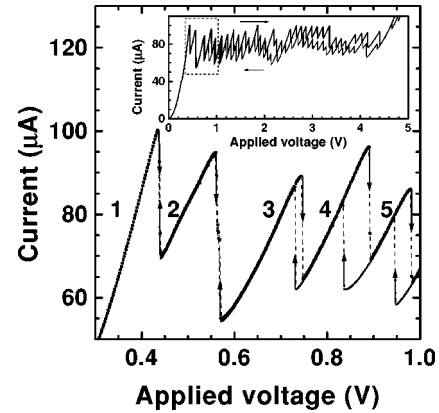


FIG. 2.  $I$ - $V$  characteristics of the first five branches (1, 2, 3, 4, and 5) for up and down sweeps, as indicated by the arrows at 5 K. Full  $I$ - $V$  characteristic for the entire first plateau and for both sweep directions are shown in the inset.

The time averaged  $I$ - $V$  characteristics are recorded using a source-measure unit (Keithley SMU 236). In all experiments, we apply a negative voltage to the top contact of the sample. The voltage steps are generated via a square-wave modulation with a period of 1 ms and a duty cycle of 50%. The length of the voltage pulse in the switching experiments is chosen to be sufficiently long to allow the field distribution inside the SL to stabilize after each voltage step in order to reset the field and charge distribution, before the next pulse arrives. The square-wave modulation and the sweeps are produced using a pulse/function generator (Wavetek 81) with a minimum ramping time of 8 ns. The current through the sample is amplified by 20 dB using the 50- $\Omega$  input of an amplifier. In the switching experiments, both the transients of the amplified current and the applied voltage are recorded at the 1-M $\Omega$  inputs of a real-time oscilloscope with a bandwidth of 1 GHz (Lecroy LC 574 AL). The voltage signal is used to trigger the measurements of the transient current response due to the voltage jumps and sweeps.

## III. $I$ - $V$ CHARACTERISTICS

The inset of Fig. 2 shows the  $I$ - $V$  characteristic of the investigated sample at 5 K for both sweep directions. The current plateau between 0.4 and 5 V originates from electric-field domain formation, where the low-field domain (LFD) is associated with hopping transport between the ground-state subband in adjacent wells and the high-field domain (HFD) corresponds to sequential resonant tunneling between the ground state of one well and the second subband in the adjacent well as described in Refs. 1 and 14. The LFD and HFD are separated by a domain boundary in the form of a charge monopole, i.e., a negative CAL. For every current jump in the up sweep, the CAL between the LFD on the emitter side and the HFD on the collector side moves by one period towards the emitter. Figure 2 depicts an enlarged section of the full  $I$ - $V$  characteristic in the inset. The variations in the current minima and maxima are due to small fluctuations (below 5%) of the doping level between the different wells.<sup>15</sup> Due to the influence of  $DX$  centers in the barrier

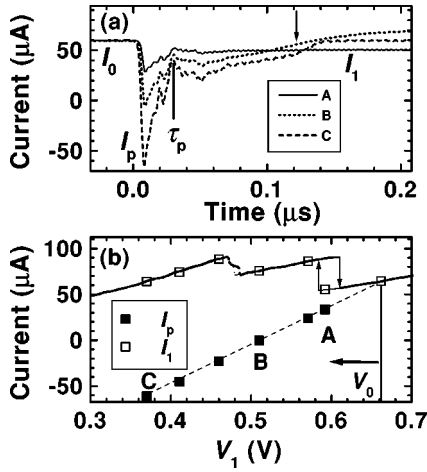


FIG. 3. (a) Averaged time traces as well as (b) peak  $I_p$  and final current  $I_1$  compared with the  $I$ - $V$  characteristics (solid line) for down jumps from the third branch to lower voltages  $V_1$  as indicated. The arrow in (a) indicates the relocation time  $\tau_{\text{reloc}}$ . The dashed line in (b) is used as a guide to the eye.

layers of the contacts, the actual voltage for a current jump may differ between different measurements, in particular after heating the sample to room temperature and cooling it again to low temperatures. Details of this effect have been described in Ref. 13.

The two-dimensional charge density  $n_{2d}$  at the domain boundary can be calculated from Poisson's equation

$$n_{2d} = \epsilon \epsilon_0 \frac{\Delta F}{e}, \quad (1)$$

where  $\epsilon$  and  $\epsilon_0$  denote the dielectric constants of the material and of the vacuum, respectively,  $\Delta F$  the electric field change at the domain boundary, and  $e$  the elementary charge. For a field-strength difference of  $\Delta F = 120 \text{ mV}/13 \text{ nm}$  and an average dielectric constant  $\epsilon \sim 12$  for GaAs and AlAs, we obtain a carrier density of  $n_{2d} = 6.1 \times 10^{11} \text{ cm}^{-2}$  for a fully developed CAL. The nominal doping density of the GaAs wells corresponds to  $n_{2d} = 1.5 \times 10^{11} \text{ cm}^{-2}$ , which is about a factor of 4 smaller than the carrier density necessary to form the domain boundary within a single well. Since the number of jumps in the  $I$ - $V$  characteristic is correlated with the number of periods, the domain boundary in the static case is formed by a CAL within a single well. In contrast, a charge depletion layer (CDL) would extend over at least four wells.

#### IV. DOWN JUMPS: MONOPOLE RELOCATION

For down jumps, the negative CAL can move according to the direction of the applied electric field. Therefore, we always expect to observe a simple monopole relocation for switching to smaller voltages. Figure 3(a) shows the current transients for a voltage jump from an initial voltage  $V_0$  on the third branch to three lower values  $V_1$ . In the first 8 ns, the current decreases due to the displacement current<sup>3,6</sup> ( $j_{\text{disp}} = \epsilon \epsilon_0 dF/dt$ ) from the initial value  $I_0$  to a downward peak value  $I_p$  given by

$$I_p = I_0 + I_{\text{disp}} = I_0 + \epsilon \epsilon_0 \frac{A}{L} \frac{dV}{dt}, \quad (2)$$

where  $A$  denotes the area of the mesa and  $L$  the length of the SL.

If  $V_0$  and  $V_1$  are on the same branch (trace A), the final current  $I_1$  is reached after  $\tau_p \approx 30 \text{ ns}$ . For jumps to other branches, the current stays after  $\tau_p$  for some time at an almost constant level (curves B and C), before it increases during a short switching time to its final value ( $I_1$ ), which is located on the down sweep characteristic. The stochastic aspects of the switching, resulting in different distribution functions, depend on the final voltage separation from the discontinuity and are described in detail in Ref. 7 for small up jumps.

Figure 3(b) shows the current value of  $I_p$  and  $I_1$  as a function of the final voltage  $V_1$ , together with the corresponding up and down sweep of the  $I$ - $V$  characteristic. While  $I_1$  just follows the down sweep of the time-averaged  $I$ - $V$  characteristic,  $I_p$  decreases linearly with decreasing  $V_1$  independently of the final current branch as described by Eq. (2). For larger down jumps,  $I_p$  can even become negative.

Amann *et al.*<sup>9</sup> and Carpio *et al.*<sup>11</sup> calculated the velocity of fully developed CAL's separating a LFD on the emitter and a HFD on the collector side as well as CDL's separating a HFD on the emitter and a LFD on the collector side as a function of the current. In the current range of the stable branches between a lower and upper critical current denoted  $I_l$  and  $I_u$ , respectively, the position of the CAL does not change. For a constant current  $I$  with  $I < I_l$  ( $I > I_u$ ), the CAL moves toward the collector (emitter), while for  $I_l < I < I_u$  it remains stationary. Near the critical current, the velocity  $v_{\text{accu}}$  of the CAL is predicted to scale as<sup>9,11</sup>

$$v_{\text{accu}} \propto \sqrt{|I - I_{l/u}|}. \quad (3)$$

However, for a CDL, the velocity  $v_{\text{depl}}$  is always positive, i.e., it always moves toward the collector. In this case,  $v_{\text{depl}}$  depends almost linearly on the current. Since we are looking at down jumps ( $I < I_l$ ), the CAL can move directly towards the collector. Therefore, the relocation of the domain boundary for down jumps is expected to be a simple motion of the CAL alone.

In Fig. 4(a), typical time traces for down jumps between two adjacent branches (curves A and B) and next-nearest-neighboring branches (curve C) are shown. After the displacement current peak, the current remains for a certain time at an intermediate level and then switches to its final value. We define a relocation time  $\tau_{\text{reloc}}$  as the time delay between the initial voltage step and the switching to the final current value. The inverse relocation time is proportional to  $v_{\text{accu}}$ . For curves A and C,  $\tau_{\text{reloc}}$  is much larger than for curve B, because  $V_1$  is close to the respective discontinuity. In Fig. 4(b), the inverse of  $\tau_{\text{reloc}}$  is shown for a down jump between adjacent branches (open dots). It has a square-root dependence on  $|V_1 - V_{th}|$ , where  $V_{th}$  denotes the voltage, at which the respective current discontinuity occurs. Since the *peak current* is a linear function of  $V_1 - V_0$  [cf. Eq. (2)], the in-

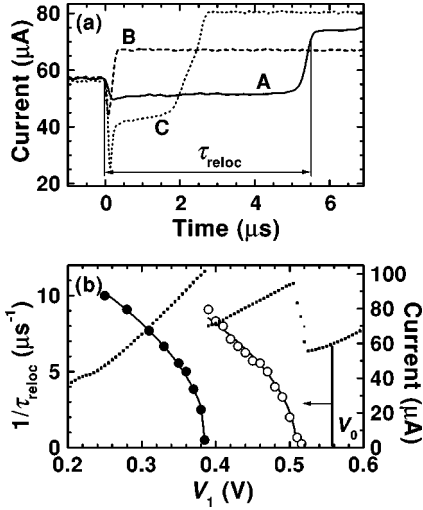


FIG. 4. (a) Typical real-time traces for jumps from the fourth to the third (A and B) branch and to the second branch (C) to define  $\tau_{reloc}$ . (b) Inverse relocation time as a function of  $V_1$  for jumps from the third to the second branch (circles) and to the first branch (dots) along with the  $I$ - $V$  characteristic (squares). The data in (b) are fitted with a square-root dependence on  $|V_1 - V_{th}|$ , where  $V_{th}$  is defined in the text.

verse relocation time is expected according to Eq. (3) to exhibit a square-root dependence on the final voltage.

For jumps between next-nearest-neighbor branches, the CAL jumps first to the adjacent well according to the intermediate current level of curve C in Fig. 4(a), before it moves with a stochastically varying delay time to its final position. This intermediate current level is below  $I_1$ , so that it is located on the unstable part of this branch, where the current decreases almost linearly with decreasing  $V_1$ . Therefore, we can also observe a square-root-like dependence of  $1/\tau_{reloc}$  as a function of the final voltage, as shown by the full dots in Fig. 4(b) for down jumps between next-nearest-neighbor branches. The situation can be generalized for down jumps between branches, which are even further apart. The CAL first moves quickly to the adjacent well of its final location and then, after a stochastically varying delay time,<sup>7</sup> jumps to its final position. We conclude that for down jumps the relocation of the domain boundary can always be described by a direct motion of the CAL alone in agreement with the theoretical predictions.<sup>9,11</sup>

## V. UP JUMPS: MONOPOLE AND TRIPOLE RELOCATION PROCESSES

For up jumps, the CAL has to move *against* the flow of the electrons. Figure 5(a) shows current traces for small up jumps (curves A and B) starting from the third branch. The peak current  $I_p$  is now larger than the initial value  $I_0$  because of the positive displacement current. Recently, we have investigated the probability distribution of the switching time for small up jumps from the third branch to the beginning of the fourth branch of the  $I$ - $V$  characteristic of this sample.<sup>7</sup> The CAL jumps after a delay time against the electron flow. For jumps to voltages far from the discontinuity, the distri-

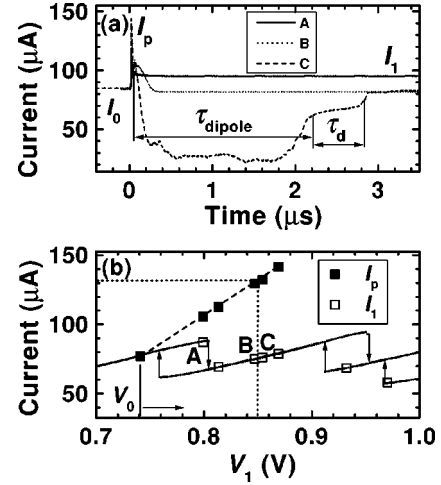


FIG. 5. (a) Real-time traces as well as (b) peak  $I_p$  and final current  $I_1$  compared with the  $I$ - $V$  characteristics (solid line) for up jumps starting from the third branch. Curves A, B, and C correspond to final voltages  $V_1 = 0.798, 0.846, \text{ and } 0.853$  V, respectively. The short-dashed line in (b) indicates the separation between the monopole and tripole relocation process, and the long-dashed line is used as a guide to the eye.

bution function of the relocation time is narrow and Gaussian. However, when the discontinuity is approached from above by reducing the  $V_1$ , the average relocation time increases by more than one order of magnitude. At the same time, the distribution function changes to a first-passage-time distribution with a steep increase for short times and a broad tail for long times.

For these small up jumps, the relocation process is very similar to the one for down jumps. After the initial peak, the current decreases slightly during a certain time interval until a critical current level is reached. Then the current decreases quickly to its final value. As for the down jumps, the inverse relocation time as defined in Fig. 4(a) also exhibits a square-root-like dependence on the final voltage  $V_1$  for these small up jumps (not shown). Figure 5(b) shows the peak  $I_p$  and final current values  $I_1$  compared with the  $I$ - $V$  characteristic. The behavior is very similar to the one for the down jump (cf. Fig. 3), taking into account the different direction of the voltage step.

For larger up jumps, the current shows a very different behavior as indicated by curve C in Fig. 5(a). After the peak, the current decreases rapidly to a range well below the stable current region of the  $I$ - $V$  characteristic. There it fluctuates around this value for a time period  $\tau_{dipole} \approx 2 \mu\text{s}$ , after which it rises to an intermediate value. It then remains for a stochastically fluctuating delay time  $\tau_d$  at this intermediate level, before it switches to its final value. Figure 5(b) shows that the final current level for larger up jumps is located on the down-sweep characteristic.

Figure 6 shows the low-current region of the transients for jumps from the third branch to the fifth branch (curve A) and from the tenth to the 13th branch (curve B). After the initial peak (region 1), a region of spikes with rather irregular amplitudes (region 2) follows, which is terminated by a larger spike. The duration of region 2 depends mainly on  $V_1$ . After

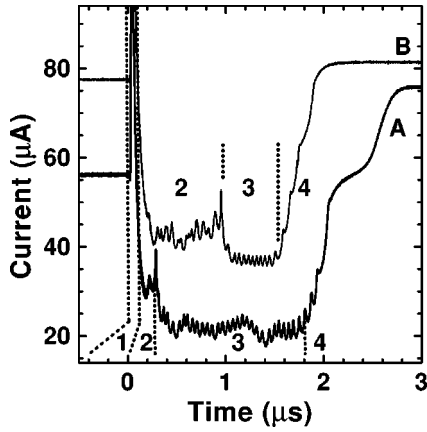


FIG. 6. Ensemble-averaged current transients for switches from the third to the fifth branch (A) and from the tenth to the thirteenth branch (B) of the  $I$ - $V$  characteristic. Curve B is shifted by a  $25\text{-}\mu\text{A}$  offset for clarity.

the larger spike, a series of regular spikes (region 3) appears with a lower current level, before the current rises (region 4). The traces are ensemble averages of about 100 measurements in order to obtain a better signal-to-noise ratio, i.e., the position of the individual spikes is essentially deterministic. However, the delay time  $\tau_d$ , defined in Fig. 5(a), fluctuates stochastically. Therefore, it is somewhat smeared out in the ensemble-averaged traces of Fig. 6.

The separation of the regular spikes in region 3 is about 50 ns, which corresponds to a frequency of 20 MHz. This frequency falls into the same range of frequencies for the spikes present in current self-oscillations of 10–20 MHz, which have been observed in the same sample for opposite polarity.<sup>16–18</sup>

We have performed several sets of measurements to vary the number of regular spikes in regions 3 and 4. For each set, we select the starting voltage  $V_0$  on a particular initial branch ( $N_0$ ) and vary the final voltage  $V_1$  to lie on different final branches ( $N_1$ ) of the  $I$ - $V$  curve. In these measurements, the number of regular spikes  $N_{rs}$  in regions 3 and 4 can be estimated by

$$N_{rs} \approx N_{SL} - N_0 - N_1, \quad (4)$$

as long as  $N_0 + N_1 < N_{SL}$ . The difference between the left- and right-hand sides of Eq. (4) varies typically between 1 and 3. For jumps with  $N_0 + N_1 > N_{SL}$ , regions 3 and 4 are not observed.

According to the theoretical work by Amann *et al.*,<sup>9</sup> the larger up jumps exhibit a more complex relocation scenario. In order to understand this behavior, we have to consider the electronic transport between the emitter contact and the first SL barrier. The emitter is assumed to be Ohmic, with an effective contact resistance  $\rho_{emitter} > 0$ . Its current-field characteristic crosses the current-field characteristic for a homogeneous field distribution of the SL in the negative-differential-resistance (NDR) region at a certain critical current level  $I_{crit}$  (cf. Fig. 1 in Ref. 9). Before the voltage step is applied, a CDL is present between the emitter and the first SL period according to Poisson's equation, since the

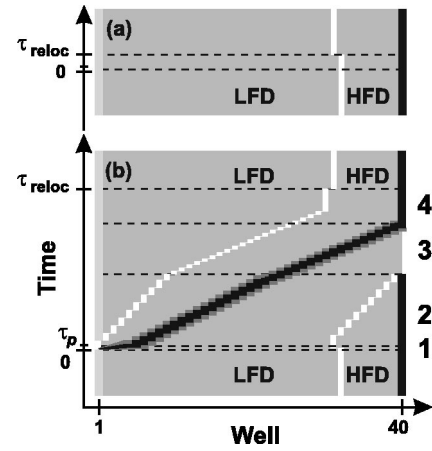


FIG. 7. Schematic evolution of the electron densities in the quantum wells during the switching process via (a) the simple monopole and (b) the tripole relocation process for a jump from the eighth to the ninth branch. The CAL's (CDL's) are indicated by white (black) areas. The emitter (collector) is located near well 1 (40). The numbers 1, 2, 3, and 4 on the right-hand side in (b) refer to the time intervals labeled in the same way in Fig. 6.

field in the low-field domain is smaller than in the emitting contact. This CDL contains a much lower carrier density than the one at the domain boundary, since the field change between the emitter and LFD of the SL is much smaller than that between the LFD and HFD. After applying the voltage step, we have to distinguish the following cases. As long as  $I_p < I_{crit}$ , this CDL persists. However, when  $I_p$  becomes larger than  $I_{crit}$ , the current in the emitter becomes larger than that in the SL. For very short current peaks, the critical value  $I_{crit}$  can be exceeded without producing a traveling CDL, since there is not sufficient time to convert the CDL into a CAL. However, for sufficiently long current peaks, the CDL between the emitter and LFD can be transformed into a CAL. At the same time, a CDL is formed between the first and second barriers of the SL, which will immediately begin to move into the SL. As the CDL moves into the SL, the new CAL between the emitter and the first barrier will also start to move into the SL. In this case, the relocation process involves two CAL's and one CDL, which we will refer to as a *tripole*.

Figures 7(a) and 7(b) show the electron densities as a function of time and space for the simple monopole and tripole relocation processes, respectively. White and black areas depict CAL's and CDL's, respectively. The four regions of the tripole relocation process defined in Fig. 6 are also indicated. The simple monopole relocation displayed in Fig. 7(a) refers to a small up jump. The larger up jumps contain four regions, which correspond to four different phases of the tripole relocation process. Phase 1 occurs during the initial displacement current peak. During this time, the CAL between the LFD and HFD moves upstream toward its final position. At the same time, the CDL at the emitter begins to move as described above, leaving a HFD behind, which grows with increasing time [cf. region 1 in Fig. 7(b)]. Since the number of periods in the HFD increases, while the applied voltage remains constant, the effective field strengths in

the LFD and HFD decrease so that the current is reduced according to the homogeneous current-field characteristic.

Phase 2 begins after  $\tau_p$ , when the current has dropped below  $I_l$ . At this point in time, there are three traveling layers separating the field in the SL into two LFD's and two HFD's [cf. region 2 in Fig. 7(b)]. Both CAL's move with the same velocity toward the collector (cf. Ref. 9). Because of the constant total voltage, the number of periods in the HFD's must now remain constant. Therefore, the sum of the velocities of the two CAL's has to be the same as the velocity of the CDL, i.e.,  $2 v_{\text{accu}} = v_{\text{depl}}$ . Since the average current should have a value for which the CDL has twice the velocity of the CAL's,<sup>9</sup> a rather low current value is observed in Fig. 6. The jumps of the two CAL's across individual quantum wells appear as irregular spikes within region 2 in Fig. 6, so that they seem to be uncorrelated.

After the original CAL reaches the collector, which is indicated by a larger spike in Fig. 6, the tripole reduces to a dipole and phase 3 begins [cf. region 3 in Fig. 7(b)]. The velocities of the CAL and CDL are now the same. Since the CDL is extended over several periods, the current transients are dominated by the motion of the CAL, which now appears as regular spikes in Fig. 6. When the CDL reaches the collector (after the time  $\tau_{\text{dipole}}$ ), phase 3 is completed.

In phase 4, only a CAL is present in the SL. Since now the number of periods in the HFD decreases with increasing time, the field strengths of LFD and HFD have to increase, resulting in an increase of the current. The CAL continues to move toward its final position. After reaching the well adjacent to its final position, the situation becomes exactly the same as for the down jumps discussed above. The current remains for a stochastically varying delay time  $\tau_d$  in this well, where  $\tau_d$  depends in the same way on the voltage to the current discontinuity, as discussed in Ref. 7. Therefore, the described behavior also explains the observation in Fig. 5 that even for larger up jumps the final current level is located on the down-sweep characteristic.

We would like to point out that this complex relocation scenario for larger up jumps may occur only in the first plateau of the  $I$ - $V$  characteristic. The current-field characteristic of the emitter contact may cross the NDR region of the first resonance, but not of any higher resonance. Under this condition, the tripole relocation process is only observed for the first plateau.

## VI. MEASUREMENTS WITH DIFFERENT TYPES OF VOLTAGE STEPS

For fast voltage steps ( $\Delta t \approx 8$  ns), the displacement current peak can be well above  $I_{\text{crit}}$ . When the step is replaced by a ramp with a certain length  $\Delta t$ , the displacement current peak will be reduced according to Eq. (2). For very long ramping times, it will fall below  $I_{\text{crit}}$ , so that the CDL cannot be formed. Figure 8 shows the current transients for jumps from the third to the fourth branch for  $\Delta t$  being varied between 10 and 120 ns. For short ramping times,  $I_p$  is large, resulting in the formation of the CDL. With increasing ramping time,  $I_p$  decreases. For  $\Delta t = 60$  ns, the formation of the CDL seems to be delayed. In this case,  $I_p = 110$   $\mu\text{A}$ , which

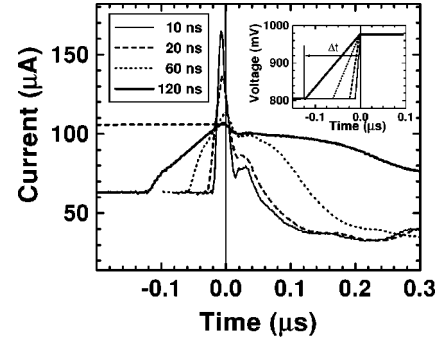


FIG. 8. Ensemble-averaged current traces for sweeps from the third to the fourth branch with different ramp times depicted in the inset. Below a certain peak current (horizontal dashed line), the relocation process changes from a tripole process to an ordinary monopole relocation process.

is still above  $I_{\text{crit}}$ . For an even longer ramping time ( $\Delta t = 120$  ns), the current transient changes to the type observed for simple monopole switching so that  $I_p$  has to be smaller than  $I_{\text{crit}}$ . Therefore, we can estimate  $I_{\text{crit}}$  to be about 105  $\mu\text{A}$ .

In order to obtain even more information about the value of  $I_{\text{crit}}$ , we performed triangular voltage sweeps with four different sweep rates as shown in Fig. 9. For a sweep rate of 10  $\text{mV}/\mu\text{s}$  and below, the  $I$ - $V$  characteristic becomes very similar to the one for dc measurements (thin lines in Fig. 9). However, with increasing sweep rate, the jumps to the next branches occur at higher (lower) voltages for the up (down) sweep so that these jumps take place at higher (lower) current levels. This observation implies that the monopole at the domain boundary cannot follow the voltage sweep anymore, because it needs a certain time to jump from one well to the adjacent well. In the depicted range of sweep rates, the displacement current  $I_{\text{disp}}$  is below 1  $\mu\text{A}$  and can therefore be neglected.

At a sweep rate of 300  $\text{mV}/\mu\text{s}$  [cf. Fig. 9(b)], the current of the 11th branch reaches  $I_{\text{crit}}$ , triggering the formation of a CDL. This can be seen from the strongly reduced current in comparison to the case with lower sweep rates. When the sweep rate is increased further,  $I_{\text{crit}}$  can already be reached on the eighth branch. This observation is an indication that  $I_{\text{crit}}$  does not depend on the actual current maximum of each

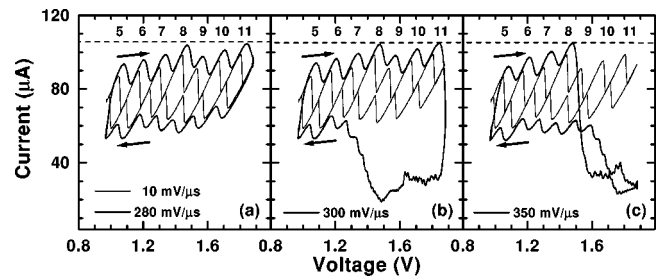


FIG. 9. Current vs voltage for triangular voltage sweeps from the fifth to the twelfth branch for different sweep rates (a) 280  $\text{mV}/\mu\text{s}$ , (b) 300  $\text{mV}/\mu\text{s}$ , and (c) 350  $\text{mV}/\mu\text{s}$  in comparison with a low sweep rate of 10  $\text{mV}/\mu\text{s}$ . If the critical current ( $I_{\text{crit}} = 105$   $\mu\text{A}$ ) is reached, the tripole process begins.

branch, but is a constant for all branches. However, for the opposite polarity, the value of  $I_{\text{crit}}$  appears to be smaller. This is probably due to a different resistance of the emitter contact. Since in this case  $I_{\text{crit}}$  seems to be even smaller than the current level of the static branches, the current becomes unstable, performing self-sustained oscillations.<sup>17</sup>

The theoretical model of Amann *et al.*<sup>10</sup> predicts that, for triangular up sweeps, the amplitude of the branches is reduced with an increasing sweep rate. At the same time, the current level increases. This result is in agreement with our observations. For a very large sweep rate, the static pattern completely disappears, indicating the formation of a CDL. The resulting critical current is about a factor of 2 larger than the maximum dc current level of the branches. This is in strong contrast to the current levels in our experiments, in which  $I_{\text{crit}}$  is only 20% larger than the maximum dc current level of the branches. Therefore, we cannot observe the final state described in the theoretical work for very large sweep rates.

## VII. CONCLUSION

The domain boundary in doped, weakly coupled SL's can relocate by both deterministic and stochastic mechanisms. For down jumps and sufficiently small up jumps, the CAL

simply moves with and against the flow of electrons, respectively. The velocity of the domain boundary has a square-root dependence on the voltage step, which can be related to the current value, in agreement with recent theoretical models. For larger up jumps, a CDL is formed at the emitter contact, which moves into the SL, producing a second CAL behind it. The relocation of the domain boundary becomes in this case a rather complex process with a tripole inside the SL, until the original CAL disappears in the collector contact. The CDL travels through the whole SL, followed by the new CAL (dipole), until the CDL also reaches the collector contact. After the new CAL has reached the well adjacent to its final position, the motion is identical to the simple monolayer relocation for down jumps. Whether this CDL appears at the emitter contact or not depends on the resistance of the emitter contact.

## ACKNOWLEDGMENTS

The authors would like to thank A. Fischer for sample growth, as well as A. Amann, A. Carpio, and L. L. Bonilla for stimulating discussions. One of us (S.W.T.) would like to thank the Paul Drude Institute for their hospitality. Partial support of the Deutsche Forschungsgemeinschaft within the framework of Sfb 296 is gratefully acknowledged.

\*Electronic address: htg@pdi-berlin.de

<sup>1</sup>H. T. Grahn, R. J. Haug, W. Müller, and K. Ploog, *Phys. Rev. Lett.* **67**, 1618 (1991).

<sup>2</sup>L. L. Bonilla, in *Nonlinear Dynamics and Pattern Formation in Semiconductors and Devices*, edited by F. J. Niedernostheide (Springer-Verlag, Berlin, 1995), Chap. 1.

<sup>3</sup>J. Kastrup, F. Prengel, H. T. Grahn, K. Ploog, and E. Schöll, *Phys. Rev. B* **53**, 1502 (1996).

<sup>4</sup>Y. Shimada and K. Hirakawa, *Jpn. J. Appl. Phys.* **36**, 1944 (1997).

<sup>5</sup>F. Prengel, A. Wacker, G. Schwarz, E. Schöll, J. Kastrup, and H. T. Grahn, *Lith. Phys. J.* **35**, 404 (1995).

<sup>6</sup>K. J. Luo, H. T. Grahn, and K. H. Ploog, *Phys. Rev. B* **57**, R6838 (1998).

<sup>7</sup>M. Rogozia, S. W. Teitworth, H. T. Grahn, and K. H. Ploog, *Phys. Rev. B* **64**, 041 308(R) (2001).

<sup>8</sup>A. Carpio, L. L. Bonilla, A. Wacker, and E. Schöll, *Phys. Rev. E* **61**, 4866 (2000).

<sup>9</sup>A. Amann, A. Wacker, L. L. Bonilla, and E. Schöll, *Phys. Rev. E* **63**, 066 207 (2001).

<sup>10</sup>A. Amann, A. Wacker, L. L. Bonilla, and E. Schöll, in *Proceedings of the 25th International Conference on the Physics of*

*Semiconductors*, edited by N. Mimura and T. Ando (Springer-Verlag, Berlin, 2001), p. 801.

<sup>11</sup>A. Carpio, L. L. Bonilla, and G. Dell'Acqua, *Phys. Rev. E* **64**, 036 204 (2001).

<sup>12</sup>H. T. Grahn, in *Semiconductor Superlattices* (World Scientific, Singapore, 1995), p. 160.

<sup>13</sup>M. Rogozia, P. Krispin, and H. T. Grahn, *J. Appl. Phys.* **90**, 4560 (2001).

<sup>14</sup>J. Kastrup, H. T. Grahn, K. H. Ploog, F. Prengel, A. Wacker, and E. Schöll, *Appl. Phys. Lett.* **65**, 1808 (1994).

<sup>15</sup>M. Patra, G. Schwarz, and E. Schöll, *Phys. Rev. B* **57**, 1824 (1998).

<sup>16</sup>Y. Zhang, R. Klann, K. H. Ploog, and H. T. Grahn, *Appl. Phys. Lett.* **69**, 1116 (1996).

<sup>17</sup>J. Kastrup, R. Hey, K. H. Ploog, H. T. Grahn, L. L. Bonilla, M. Kindelan, M. Moscoso, A. Wacker, and J. Galán, *Phys. Rev. B* **55**, 2476 (1997).

<sup>18</sup>J. W. Kantelhardt, H. T. Grahn, K. H. Ploog, M. Moscoso, A. Perales, and L. L. Bonilla, *Phys. Status Solidi B* **204**, 500 (1997).